



## Effect of Doped Nitrogen on the Crystallization Behaviors of Ge<sub>2</sub>Sb<sub>2</sub>Te<sub>5</sub>

Inseok Yang, Kihoon Do, Hyun-Jin Chang, Dae-Hong Ko, and Hyunchul Sohn<sup>z</sup>

Department of Materials Science and Engineering, Yonsei University, Seoul 120-749, Korea

The crystallization behaviors of Ge<sub>2</sub>Sb<sub>2</sub>Te<sub>5</sub> and nitrogen-doped Ge<sub>2</sub>Sb<sub>2</sub>Te<sub>5</sub> films, deposited by dc magnetron sputtering, were investigated using the in situ resistance measurement, X-ray diffractometry, and transmission electron microscopy (TEM). The kinetic constants were estimated using the classical Johnson–Mehl–Avrami–Kolmogorov model from the resistance measurement of Ge<sub>2</sub>Sb<sub>2</sub>Te<sub>5</sub> and nitrogen-doped Ge<sub>2</sub>Sb<sub>2</sub>Te<sub>5</sub> films. The nitrogen-doped Ge<sub>2</sub>Sb<sub>2</sub>Te<sub>5</sub> showed a one-step process with the Avrami constant (*n*) of 1, while the Ge<sub>2</sub>Sb<sub>2</sub>Te<sub>5</sub> thin film showed a two-step transformation with *n* of 3.6 and 1. The cross-sectional TEM revealed that the crystallizations were concentrated to the regions of 20–30 nm near the top surfaces rather than occurring throughout the films of Ge<sub>2</sub>Sb<sub>2</sub>Te<sub>5</sub> and nitrogen-doped Ge<sub>2</sub>Sb<sub>2</sub>Te<sub>5</sub> films. The annealed Ge<sub>2</sub>Sb<sub>2</sub>Te<sub>5</sub> showed continuous crystalline films with 20 nm grains at the surface in conjunction with the saturation of the sheet resistance, while the annealed nitrogen-doped Ge<sub>2</sub>Sb<sub>2</sub>Te<sub>5</sub> showed nanocrystalline phases with 5 nm grains near the surface with a continuous decrease in sheet resistance. The crystallization of nitrogen-doped Ge<sub>2</sub>Sb<sub>2</sub>Te<sub>5</sub> was observed to be a nucleation-dominant process, while that of Ge<sub>2</sub>Sb<sub>2</sub>Te<sub>5</sub> was a growth-dominant process.

© 2010 The Electrochemical Society. [DOI: 10.1149/1.3321759] All rights reserved.

Manuscript submitted July 24, 2009; revised manuscript received January 20, 2010. Published March 11, 2010.

Recently, phase-change random access memory (PRAM) has drawn much attention as a promising candidate for the next-generation nonvolatile memory devices because of its nonvolatility, low operation power, fast data access, good repeatability, compatibility with the complementary metal oxide semiconductor process, and high scalability.<sup>1,2</sup> Ge<sub>2</sub>Sb<sub>2</sub>Te<sub>5</sub> (GST), which has been the most widely investigated film for the PRAM application, shows a fast and reversible phase transition, which is desirable for memory application. However, the realization of PRAM is hampered by issues such as the high reset current and the potential thermal cross-talk among neighboring cells in high density memory devices. To cope with such issues, various research groups investigated the doping effect of nitrogen on the material properties of GST. Nitrogen doping into GST was very effective in modifying the crystallization temperature and electrical properties by the suppression of crystallization.<sup>3–5</sup> Although several research groups have reported the phenomena of improvements in characteristics, the fundamental behavior of nitrogen is still not clear. Even the exact nature of incorporated nitrogen such as the chemical state is not yet examined clearly.<sup>6–10</sup> However, the realization of PRAM with GST requires the profound understanding of the kinetics of the phase transition and the relationship between the structural transition and the resistivity change during the phase transition.

In this work, the crystallization kinetics of nitrogen-doped GST (NGST) thin films, deposited by dc magnetron sputtering, was investigated in comparison with that of GST films using the in situ resistance measurement, X-ray diffractometry (XRD), and transmission electron microscopy (TEM).

### Experimental

The GST and NGST films with a thickness of 180 nm were deposited on glass substrates using a Ge<sub>2</sub>Sb<sub>2</sub>Te<sub>5</sub> target by dc magnetron sputtering at room temperature. First, the glass substrates were chemically cleaned to remove organic contaminants. The base pressure and the working pressure for the GST sputtering were  $1 \times 10^{-7}$  Torr before the deposition and 1.0 mTorr with an Ar flow rate of 3.0 sccm during sputtering. A mixture of N<sub>2</sub> and Ar gases was used for the deposition of NGST with a nitrogen flow rate of 0.2 sccm and an Ar flow of 2.8 sccm. The nitrogen compositions of NGST were estimated to be 10 atom % by Rutherford backscattering.

To investigate the kinetics of the phase transformation, the GST and NGST samples were placed on the quartz plate and annealed by

halogen lamps located on the upper and lower sides of the samples. The GST and NGST samples were heated to the predetermined temperatures by the rate of 3°C/min, and the resistance of the samples was measured in situ and in real time during the subsequent isothermal annealing under N<sub>2</sub> ambient of 1.0 Torr to prevent the surface oxidation.

The crystalline structures were analyzed by XRD with Cu K $\alpha$  of  $\lambda = 1.541 \text{ \AA}$  after isothermal annealing with scanning from 20 to 45°. Also, the microstructures of the samples were investigated by cross-sectional TEM using JEOL JEM 2100F with a field emission gun operated at 200 kV.

### Results and Discussion

The sheet resistances of the GST and NGST films were measured in real time as the function of annealing time at various temperatures in an in situ resistance measurement system to investigate the crystallization behavior of those films. In our work, the annealing temperatures were chosen so that the changes in the sheet resistances occurred in the time span between 10<sup>2</sup> and 10<sup>3</sup> s during isothermal annealing. From the pretest, the GST films were annealed isothermally at temperatures of 139, 142, and 145°C and the NGST films were annealed at temperatures of 179, 182, and 185°C, which were 40°C higher than the annealing temperatures of GST.

Figure 1 shows the change in the sheet resistance of the GST and NGST films isothermally annealed at various temperatures. The GST films showed an abrupt decrease in sheet resistances in the relatively small time span. Such reduction in sheet resistance in the GST films were attributed to the crystallization of the amorphous phase into the face-centered cubic (fcc) crystalline phase.<sup>11</sup> The incubation time to the resistance reduction was decreased from about 500 to 100 s as the annealing temperature was increased from 139 to 145°C. However, the NGST films showed much higher resistances before and after annealing than the GST films even for annealing at temperatures that were 40°C higher than the annealing temperatures of GST. The reduction in resistance in the NGST films occurred at higher annealing temperatures with a slower rate than the GST films, suggesting that the crystallization rate of NGST was lower than that of GST films probably due to the incorporated nitrogen.

To examine the different crystallization kinetics between GST and NGST systems, a reasonable estimation of the crystalline fraction  $\chi$  should be required to analyze in the kinetic view. By employing a simple crystallization model, the crystalline volume fraction of GST and NGST was calculated by measuring the change in the sheet resistance. To estimate the crystallization behavior, the general numerical calculations, such as the Wiener upper bound model, the Wiener lower bound model, and the effective medium approximation, are used to describe the relationship between the physical prop-

<sup>z</sup> E-mail: hyunchul.sohn@yonsei.ac.kr

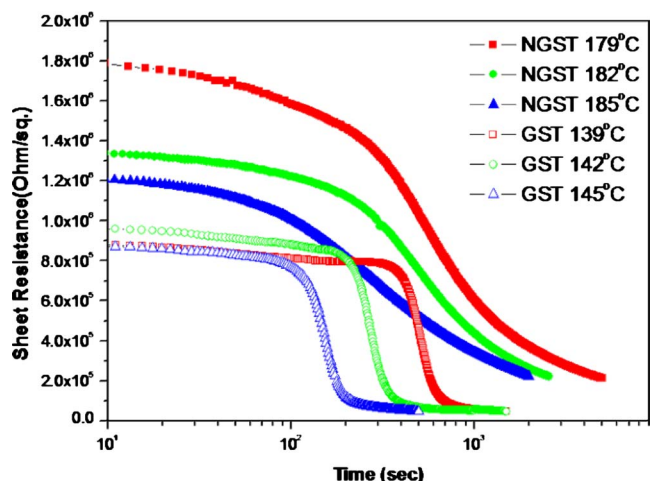


**Figure 1.** (Color online) The real time variation in sheet resistance of GST and NGST films measured in situ during isothermal annealing.

erties and the volume fraction of the crystalline.<sup>12</sup> Contrary to the optical properties, the electrical conductivity shows a strong deviation from a linear dependency on the crystallinity due to the percolation effect. However, in GST, the experimental results agree well with the calculation of the Wiener upper bound model.<sup>12</sup> Therefore, we employed the Wiener upper bound model to estimate  $\chi$ , which is given by

$$\chi = \frac{R_c(R_a - R)}{R(R_a - R_c)} \quad [1]$$

where  $R$ ,  $R_a$ , and  $R_c$  are the sheet resistances of measured value, amorphous, and crystalline phases, respectively.

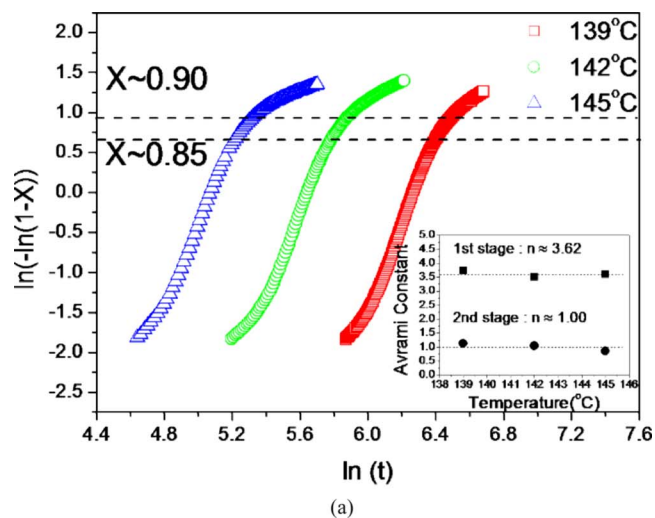
The Johnson–Mehl–Avrami–Kolmogorov (JMAK) curve corresponding to each isothermal annealing is plotted in Fig. 2a and b to investigate the crystallization behavior of the amorphous GST and NGST. The analysis of GST films showed that the Avrami constant was changed from 3.6 to 1.0, implying a two-step kinetics of the crystallization. The examination on the JMAK plots revealed that the Avrami constant was changed to 1.0 of the second stage of crystallization at the crystalline volume fractions of 85–90% during the isothermal annealing.

Such two-step kinetics of the crystallization for GST was also reported by others.<sup>13,14</sup> The changes in  $n$  values were considered as the different crystallization mechanisms or dimensional growths in the lateral and vertical directions. Also, Ruitenber et al. suggested that the buckling of the JMAK plot can be the result of the difference in film geometry or incubation time in each case.<sup>15</sup>

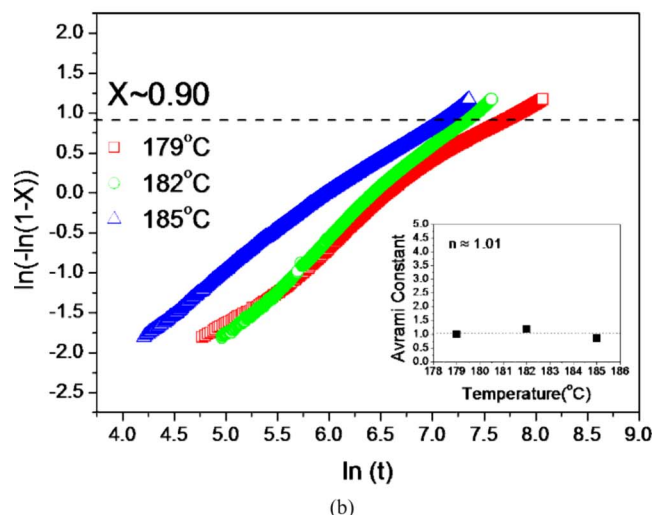
In general, the Avrami constant ( $n$ ) provides the information on the mechanism of phase transformation and can be expressed in the form below

$$n = am + b \quad [2]$$

where  $a$ ,  $b$ , and  $m$  are the indexes of growth, nucleation, and dimension of growing.<sup>15,16</sup> The Avrami constant of 3.62, assuming 4 at the first stage of the GST crystallization, suggests that the crystallization occurred with the constant nucleation and growth rates and that the growth proceeded in three dimensions. Moreover, the activation energy for GST crystallization in the first stage was estimated to be 2.19–2.21 eV, which agrees with the work reported by Ryu et al.<sup>17</sup> and Yamada et al.<sup>18</sup> The average Avrami constant of 1.0 at the second stage of the crystallization was considered to imply one-dimensional grain growth without additional nucleation. Although the activation energy at the second stage is smaller than that in the first stage, it shows the limitation to describe the initial crystallization of GST due to such geometrical restrictions.



(a)



(b)

**Figure 2.** (Color online) (a) JMAK plots of GST for isothermal annealing at 139, 142, and 145°C and corresponding Avrami constants as a function of temperature shown in the inner box. (b) JMAK plots of NGST for isothermal annealing at 179, 182, and 185°C, and corresponding Avrami constants as a function of temperature shown in the inner box.

The JMAK equation for the crystallization of GST conducted in this work was expressed as follows

$$X(T, t) = 1 - \exp \left\{ - \left[ (1.79 \times 10^{24}) \exp \left( - \frac{2.20 \text{ eV}}{k_B T} \right) t \right]^{3.62} \right\} \quad [3]$$

The average Avrami constant of NGST films was estimated to be about 1.0 from the linear regression analysis throughout the whole transformation, as shown in Fig. 2b. No changes in the Avrami constant were observed up to 90% crystallization of the amorphous NGST films, indicating that the phase transformation mechanism in NGST did not vary until the crystallization was almost finished. Considering the fact that the Avrami constant was close to 1 and that the growth of the crystalline phases would proceed in three dimensions initially like GST, both nucleation index  $b$  and growth index  $a$  were expected to be less than 1, which implied that the nucleation rate and the growth rate of crystalline phases were decreased with increasing annealing time.

The activation energy for the crystallization of NGST films was estimated to be 2.71–2.81 eV with an average of 2.76 eV, which was

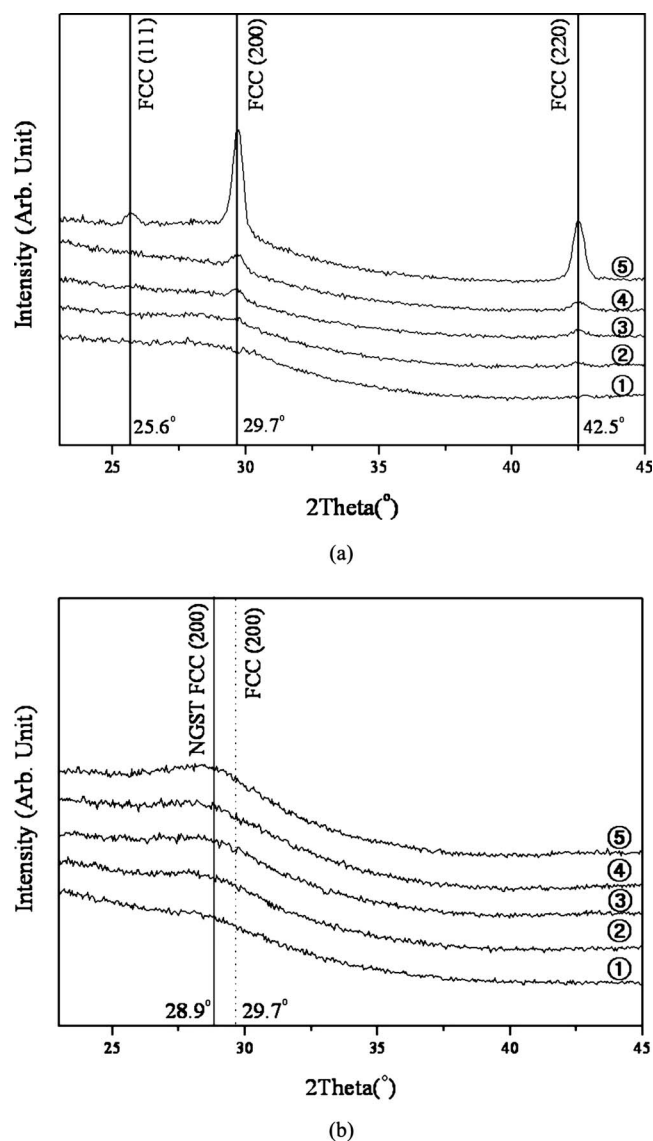


**Figure 3.** (a) XRD spectra of GST thin films annealed at 142°C for ~0, ~222, ~266, ~288, and ~1500 s, and (b) XRD spectra of NGST thin films annealed at 182°C for ~0, ~435, ~661, ~1310, and ~2560 s.

about 0.56 eV larger than that of GST. The JMAK equation for NGST crystallization in this work was expressed as follows

$$X(T,t) = 1 - \exp\left\{-\left[(5.00 \times 10^{27})\exp\left(-\frac{2.76 \text{ eV}}{k_B T}\right)t\right]^{1.01}\right\} \quad [4]$$

According to the different kinetic values such as the activation energy, the Avrami exponent, and the effective rate constant between GST and NGST, as expressed in Eq. 3 and 4, NGST requires an annealing temperature about 50°C higher than GST to achieve the same fraction of crystallization for the same annealing time.

The crystalline structures of the GST and NGST films isothermally annealed at 142 and 182°C were studied by XRD. Although the estimated JMAK equations in this work describe the crystallization kinetics, only the Avrami constant  $n$  shows the limitation to determine the exact crystallization behavior alone because  $n$  can be a combination of  $a$ ,  $b$ , and  $m$  values. For further investigation of the crystallization kinetics, we analyzed the crystalline structure and microstructure of grains. Figure 3a shows the XRD spectra of the as-deposited and the annealed GST samples with annealing times of

200–1500 s, where the resistance decrease was observed in the in situ resistance measurement. No crystalline XRD peak was observed in the as-deposited GST films, indicating an initial amorphous state of the GST film. The crystalline peaks of (111), (200), and (220) of fcc GST showed up after annealing for more than 200 s, and their intensities were increased with increasing annealing time. However, no XRD peak of the stable hexagonal structure was observed even after annealing for 1500 s.

Figure 3b shows the XRD spectra from the as-deposited and the annealed NGST films for annealing times of 435–2560 s. No XRD peak was observed from the as-deposited NGST films. NGST films did not show any distinctive crystalline XRD peak but a broad peak at 29° even after annealing for 2560 s.

By using Scherrer's equation, the grain sizes of GST and NGST films were estimated from the full width at half-maximum (fwhm) of (200) peaks. The grain size of the GST films annealed for 1500 s was estimated to be 18.3 nm, and that of the NGST films annealed for about 2600 s was 3.3 nm, which was more than five times smaller than the grain size of GST films. The reduced grain size of annealed NGST films was reported to be due to the suppression of grain growth.<sup>9,10</sup>

The microstructures of GST and NGST films were investigated by the cross-sectional TEM. Figure 4a shows the cross-sectional TEM images of the GST thin film annealed at 142°C for 1000 s. Even though the full crystallization of GST was expected from the saturation of the measured resistance after annealing for 500 s, the TEM images showed that the continuous crystalline GST is only near the surface in GST films annealed by a halogen lamp. The thickness of the crystallized region of GST was estimated to be about 20 nm. It is concluded that the in situ resistance measurement gave the information of the crystallization only at the thin surface region of GST films. Although the crystalline GST has low resistivity, the linking of the fcc GST grains is considered to produce the resistivity saturation, and the growth of crystalline GST films in the direction perpendicular to the surface produced further reduction in the resistivity with increasing annealing time shown in Fig. 1. Apparently, the crystallization of GST films is proceeded by the heterogeneous nucleation at the surface and subsequent growth during the isothermal annealing between 139 and 145°C.

The thickness of the crystallized region and the average grain size in GST films were estimated to be about 20 nm from cross-sectional TEM, as shown in Fig. 4a. To analyze the microstructure of GST films, the rectangular region with a dotted line was observed with high magnifications. The high resolution transmission electron microscopy (HRTEM) image at the bottom in Fig. 4a, shows lattice images of the crystallized GST grain with interplanar spacings of 3.05, 3.05, and 2.12 Å, which corresponded to (200), (020), and (220) planes of fcc GST, respectively.

Figure 4b shows the cross-sectional TEM images with various magnifications of NGST thin films annealed at 182°C for 2000 s. The TEM image shows the high density of nanocrystallines in the region of about 30 nm from the surface of NGST films. The crystalline NGST grain was observed to be smaller in size but higher in density than those of crystalline GST. The HRTEM image of the region with dotted lines in the NGST grains shows that the interplanar spacings of (200), (020), and (220) planes were measured to be about 3.11, 3.10, and 2.17 Å, respectively, which were 0.05–0.06 Å larger than those of GST. Such increases in interplanar spacings agree very well with the previous observation made by Jeong et al.<sup>3</sup>

Table I summarizes the comparison of grain density and size in the crystallized GST and NGST films after isothermal annealing. The linear grain density, which is defined as the number of grains per unit length, was estimated to be a few hundred per micrometer in crystallized NGST. The grain size of crystallized NGST was five times smaller in diameter and ten times larger in linear grain density than that of GST, which indicated that the crystallization in NGST was nucleation-process dominant. Such high density and small grain size in NGST films were considered to be due to the doped nitrogen

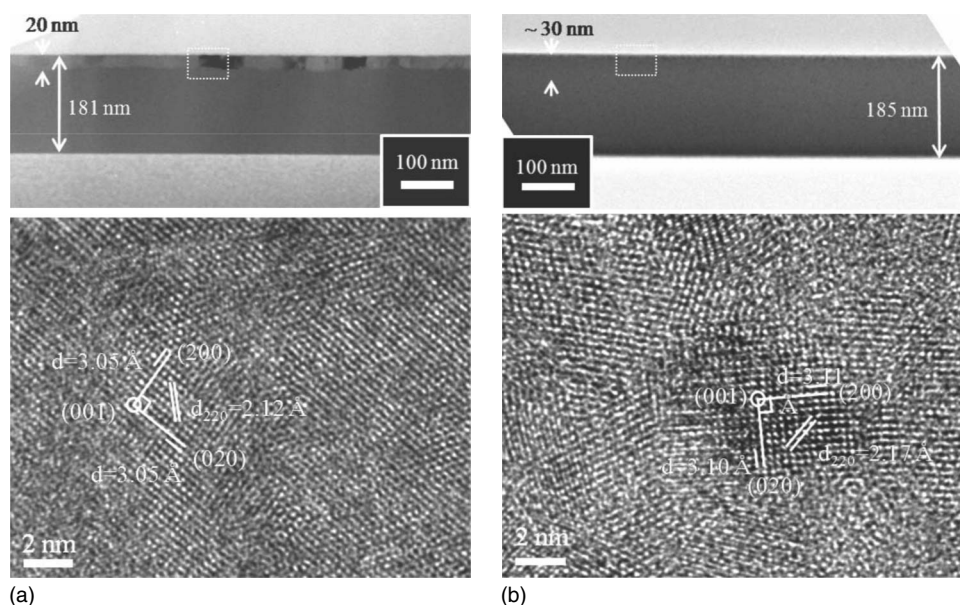


**Figure 4.** Cross-sectional TEM images of (a) GST thin films annealed at 142°C for 1000 s and (b) NGST thin films annealed at 182°C for 2000 s. The high resolution pictures at the lower parts of (a) and (b) are the magnified images taken from the regions marked by dotted lines in the images above.

in the NGST thin film, which suppressed the grain growth by disturbing the rearrangement of Ge, Sb, Te atoms, requiring a higher activation energy with longer crystallization time.

### Conclusion

In summary, the crystallization behavior of GST and NGST films were investigated using an in situ resistance measurement during isothermal annealing by halogen lamp, XRD, and cross-sectional TEM. The analysis of the sheet resistance measured in situ showed that the GST thin films were crystallized in a two-step process with the Avrami constants of 3.6 and 1, while the NGST thin films crystallized by a one-step process with  $n$  of 1. However, the cross-sectional TEM revealed that the crystallizations were concentrated to the regions of 20–30 nm near the surface for the GST and NGST films rather than throughout the whole films. Annealed  $\text{Ge}_2\text{Sb}_2\text{Te}_5$  showed the continuous crystalline phase at the surface with grains of 20 nm in conjunction with the saturation of the sheet resistance, while the annealed nitrogen-doped  $\text{Ge}_2\text{Sb}_2\text{Te}_5$  showed nanocrystalline phases with 5 nm grains near the surface without the saturation of the sheet resistance. The suppression of grain growth and the increase in the interplanar spacing were observed in NGST films by XRD and TEM analyses, which were attributed to the additional nitrogen in the GST lattice.

**Table I. Quantitative analyses of grain structures by TEM and XRD.**

Grain information		GST	NGST
Grain size (nm)	XRD fwhm	18.3	3.3
	TEM	~20	Surface: > ~ 5 Else: < 5
Distributed depth (nm)		~20	~30
Linear grain density ( $\mu\text{m}^{-1}$ )		~60	~800
d-spacing (Å): (200)	XRD peak	3.10	3.18
	TEM	3.05	3.11

### Acknowledgments

This work was supported by the next-generation growth engine project of the Ministry of Knowledge Economy.

Yonsei University assisted in meeting the publication costs of this article.

### References

- S. Tyson, G. Wicker, T. Lowrey, S. Hudgens, and K. Hunt, in *Aerospace Conference 2000*, IEEE (2000).
- S. Lai and T. Lowrey, *Tech. Dig. - Int. Electron Devices Meet.*, **2001**, 803.
- T. H. Jeong, M. R. Kim, H. Seo, J. W. Park, and C. Yeon, *Jpn. J. Appl. Phys., Part 1*, **39**, 2775 (2000).
- H. Horii, J. H. Yi, J. H. Park, Y. H. Ha, I. G. Baek, S. O. Park, Y. N. Hwang, S. H. Lee, Y. T. Kim, K. H. Lee, et al., *Dig. Tech. Pap. - Symp. VLSI Technol.*, **2003**, 177.
- R. M. Shelby and S. Raoux, *J. Appl. Phys.*, **105**, 104902 (2009).
- H. Seo, T.-H. Jeong, J.-W. Park, C. Yeon, S.-J. Kim, and S.-Y. Kim, *Jpn. J. Appl. Phys., Part 1*, **39**, 745 (2000).
- B. Liu, Z. Song, T. Zhang, J. Xia, S. Feng, and B. Chen, *Thin Solid Films*, **478**, 49 (2005).
- K. Kim, J.-C. Park, J.-G. Chung, S. A. Song, M.-C. Jung, Y. M. Lee, H.-J. Shin, B. K. Kuh, Y. Ha, and J.-S. Noh, *Appl. Phys. Lett.*, **89**, 243520 (2006).
- Y. Kim, M. H. Jang, K. Jeong, M.-H. Cho, K. H. Do, D.-H. Ko, H. C. Sohn, and M. G. Kim, *Appl. Phys. Lett.*, **92**, 061910 (2008).
- Y. Kim, U. Hwang, Y. J. Cho, H. M. Park, M.-H. Cho, P.-S. Cho, and J.-H. Lee, *Appl. Phys. Lett.*, **90**, 021908 (2007).
- K. Do, H. Sohn, and D.-H. Ko, *J. Electrochem. Soc.*, **154**, H867 (2007).
- D. Kim, F. Merget, M. Laurenzis, P. H. Bolivar, and H. Kurz, *J. Appl. Phys.*, **97**, 083538 (2005).
- T. H. Jeong, M. R. Kim, H. Seo, S. J. Kim, and S. Y. Kim, *J. Appl. Phys.*, **86**, 774 (1999).
- V. Weidenhof, I. Friedrich, S. Ziegler, and M. Wuttig, *J. Appl. Phys.*, **86**, 5879 (1999).
- G. Ruitenbergh, A. K. Petford-Long, and R. C. Doole, *J. Appl. Phys.*, **92**, 3116 (2002).
- S. Ranganathan and M. von Heimendahl, *J. Mater. Sci.*, **16**, 2401 (1981).
- S. O. Ryu, S. M. Yoon, K. J. Choi, N. Y. Lee, Y. S. Park, S. Y. Lee, B. G. Yu, J. B. Park, and W. C. Shin, *J. Electrochem. Soc.*, **153**, G234 (2006).
- N. Yamada, E. Ohno, K. Nishiuchi, N. Akahira, and M. Takao, *J. Appl. Phys.*, **69**, 2849 (1991).